WIND TUNNEL TEST OF GUST RESPONSE FOR DISTRIBUTED PROPELLER-WING CONFIGURATION

HUANG KUNHUI[1], ZHANG ZHITAO[2], LIU DAWEI[2] and XIE CHANGCHUAN[1,*]
[1] School of Aeronautic Science and Engineering, Beihang University, Beijing 100191, China
[2] China Research and Development Academy of Machinery Equipment, Beijing, 100089, China

Keywords: wind tunnel test, gust response, distributed propeller, wing deformation, aeroelasticity

Abstract: High-efficiency distributed propellers have emerged as a propulsion option for future transportation, necessitating a thorough understanding of the propellers' slipstream performance and aerodynamic interaction with a wing under a variety of operating situations. At low subsonic speed and typical rotational speed, an experimental gust wind study was carried out to examine the impacts of the distributed propellers' thrust and slipstream on a flexible wing with a 300 mm wing-chord. A fiber optic sensing system was designed and deployed on the beam surface aimed to measure the time-domain response of wingtip deformation. The results demonstrate the accuracy of the measurement system in predicting structural deformation and aerodynamic performance under various gust situations.

1 INTRODUCTION

The leading and trailing edges of wings with distributed propellers (DP) are usually designed by distributing numerous motors with propellers spanwise throughout the wing. Additionally, the suggested concept seeks to improve flight safety, noise reduction, and aerodynamic efficiency[1]. As an alternate method to improve the aircraft's flying performance by lessening the strength of the vortices and lift-induced drag, for instance, having distributed drive throughout the wing span may benefit the aerodynamic structures at the end of the wing[2]. Based on the above advantages, some distributed propeller aircraft have been designed, such as the classical NASA's Helios[3], NASA's X-57[4], and X-HALE[5]. Numerous studies have been conducted through computational fluid dynamics[6], numerical simulation approaches[7], and experiments[8], especially for NASA's X-57.

According to Nicholas et al.[9] performance projections for distributed propulsion configurations, the X-57 distributed propulsion wing performs as intended during cruise flight and meets or exceeds targets for high-lift generation during low-speed flight. It is important to note that this is the first time the large, complex tradespace of candidate geometries for the X-57 has been examined. High-lift propellers are used in the aerodynamic interaction between distributed propellers and the wing to increase dynamic pressure and alter the distribution of the local angle of attack[10]. The coupling between the propeller-induced velocity profile and wing surface affects DEP aircraft performance significantly since it changes the local upwash velocity[1]. Michael et al.[11] implemented a higher-order vortex lattice model employing distributed vorticity elements capable of capturing the distributed mutual influence between propellers and wing. A more thorough numerical analysis of a distributed propeller design explains the main components of interaction and yields informative wing-loading data[7].

The flow-field distribution and lift-drag performance of wing are altered by the distributed propellers. Larger loads operating on the wing structure generally follow higher aerodynamic performance. As a result, when conceptualizing a DP-Wing configuration, the aeroelastic characteristic should be taken into account. Teixeria et al.[12] created a more advanced nonlinear aeroelastic-coupled flight dynamics framework that is capable of calculating the aerodynamic performance of the propellers and the impact of inertia on the response of a very flexible distributed propeller aircraft. It is concluded that the propellers influence the wing equilibrium shape. Ostuka et al.[13] have a nonlinear static and dynamic analysis for a very flexible wing with distributed propellers, and the dynamic result shows that the propellers reduce the vibration amplitude mainly because the propeller-induced axial velocity enhances the aerodynamic damping. Furthermore, one significant aeroelastic manifestation of the aeroelasticity of distributed propeller aircraft is the crush of NASA's Helios. According to the engineers ' analysis, the very flexible wing is extremely vulnerable to wind gusts. An investigation reveals that the distributed concept can alleviate gust loads more effectively because it provides load redistribution from several propellers, which can help address the problem of gust load alleviation[14]. Thus, exploring the gust response of the DP-Wing configuration is very necessary.

To gain a deeper understanding of the unstable aerodynamic and aeroelasticity principles that define the DP-Wing configuration operating at varying freestream velocity, incidence angle of attack, gust amplitude, and gust frequency, a gust wind tunnel test was carried out as part of this study. In order to achieve noteworthy performance, the tested model, which has three distributed propellers/wing, operates under the aforementioned circumstances. The wind tunnel experiment used the instantaneous reaction of wingtip deformation along two directions.

2 TEST VEHICLE AND EXPERIMENT SETUP

2.1 Test vehicle

2.1.1 Propeller model

The propeller used for the wind tunnel test reported here is a two-bladed carbon fiber propeller with a diameter of 330.2 mm and a pitch of 165.1 mm, and the evolution of the chord and the pitch angle distributions of the propeller are plotted in Figure 1.

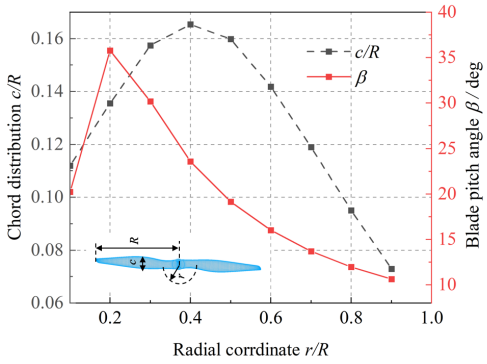

Figure 1 The chord and pitch angle distribution of the two-bladed propeller[15].

2.1.2 DP-Wing model

A flexible wing model, the parametric parameters of which are displayed in Table 1, was

created in order to examine how the gust affected the performance of the DP-Wing configuration. The rectangular wing beam is situated at the 40% chord line of the wing and measures 30 mm by 20 mm with a 1 mm thickness. It was constructed using carbon fiber to create the beam. The density of the carbon material is 0.11 kg/m^3, and the elastic modulus is 125 GPa. Eleven light 3D printed parts made of Resin-8200 make up the wing frame for the design. Each section is attached to the wing beam in a single place. The two wing portions closest to the root are clearly broader at 175 mm, whilst the remaining nine outer sections are all thinner at 145 mm. The distance, intended to be 2 mm, between consecutive wing portions received special attention. Since the theoretical dynamic analysis only included the beam effect, the gap's function in the aeroelastic test model is to eliminate the additional stiffness effect[17]. As a result, the total length of the wingspan is 1675 mm. The wing section near the root is numbered section-1, and the box mounted at the wing tip is numbered section-11. The distributed propellers are located at the middle of section-3, section-6, and section-9 along the wing span and corresponding to the spanwise locations: Y/L_w = 0.255, 0.518, and 0.781. Three nacelles are designed to contain the electric motor driving the propeller, and the six-component balance are used to measure the propeller thrust and torque. In addition, both sides of each wing section are ribs with relief holes, with a wall thickness of 2.5 mm.

Using Catia V5R21, the propeller, wing, and support stand was constructed in order to carry out the DP-Wing configuration gust test. Figure 2 displays the completed wind tunnel test model as well as the intended 3-D model.

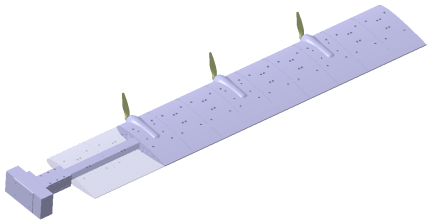

(a) 3-D Catia model

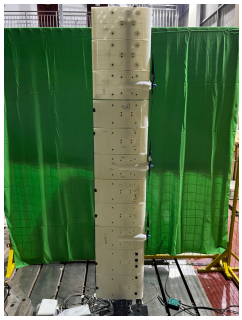

(b) wind tunnel test model

Figure 2 The flexible model of DP-Wing configuration.

Table 1 Design properties of the DP-Wing configuration.

Parameter	Value	Parameter	Value
Propeller radius	165.1 mm	Wing chord length	300 mm
Airfoil of wing	NACA0015	Elastic axis	40% chord line of wing
Wing span length	1675 mm	Cross-section of beam	30 mm × 20 mm rectangle

A number of meticulous mode tests have been conducted to create a suitable model that may cause noticeable deformation in the test operating state of the wind tunnel. Table 2 displays the primary linear modes of the DP-Wing configuration model. The first two modes had low

frequencies, and the majority of gust frequencies were clustered around these frequencies for modes 1 and 2.

Table 2 Modes of the DP-Wing configuration.

Mode	Description	Frequency (Hz)
1	1st bending mode	2.097
2	1st bending mode in-plane	2.970
3	1st torsion mode	7.730
4	2nd bending mode	13.050
5	2nd bending mode in-plane	17.810

2.2 Experimental setup and measurement techniques

2.2.1 Experimental setup

All wind tunnel gust response tests were conducted in the FD-09 low-speed wind tunnel at the China Academy of Aerospace Aerodynamics. The Reynolds number as maximum test velocity is about 1.4e+6, and the turbulence coefficient of the wind tunnel is lower than 0.1%.

An installation of a test model in the wind tunnel is presented in Figure 3. The model was attached to a vertically supported system that was mounted to the tunnel floor and coupled to an angle of attack converter. A six-component balance was attached between the DP-Wing configuration and the support system to measure the aerodynamic forces of the DP-Wing configuration. It is important to note that the support system is intended to be completely inflexible. A gust generator placed upstream in the tunnel is used to generate the anticipated gust condition for the gust test. At a distance of 600 mm, two rectangular blades with NACA0015 airfoils deflect synchronously and sinusoidally. Every blade has a span length of 2000 mm and a chord length of 300 mm. During the wind tunnel test, the DP-Wing configuration model was arranged 2250 mm away from the trailing edge of the generator blade, and the distance named L1 is also shown in Figure 3. The distance is specified as L2, and the propeller installed at section 3 is 1000 mm above the wind tunnel floor. Moreover, L3 denotes the 600 mm distance from the wind tunnel floor to the generator blade's root. Every blade has a deflection angle ranging from -7 to 7 degrees, and the frequency of the created gusts varies from 1 to 7 hertz. Ref [17] contains additional specific information about gust velocity.

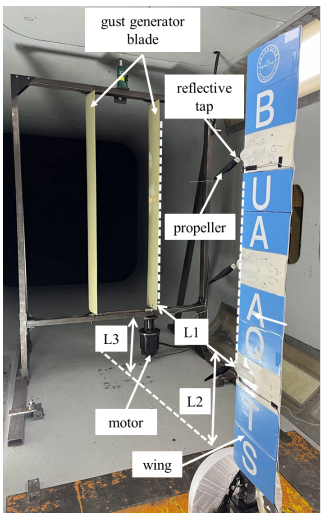

Figure 3 Wing model installation and gust generator in the wind tunnel.

2.2.2 Measurements techniques

An advanced fiber optic sensing system was used in a wind tunnel test to indirectly evaluate the response of structural deformation. As seen in Figure 4, Fiber Bragg Grating (FBG) sensors with various characteristic wavelengths are affixed to the wing beam's surface using epoxy adhesive. The strain values at various spots on the beam surface are obtained by attaching the FBG sensors to them. Next, using the Strain-Displacement Transformation (SDT) algorithm to numerically integrate the measured strains, the rotations and displacements of the wing beam along the wing span are calculated[18].

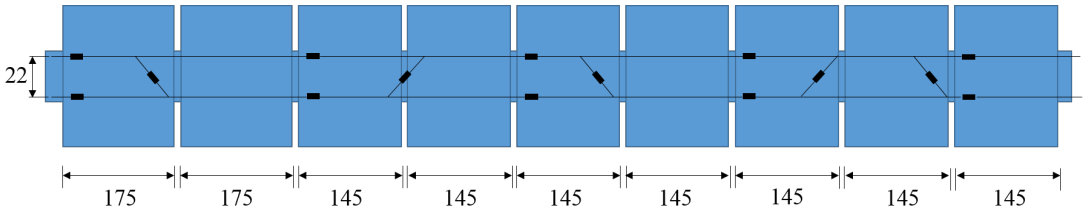

Figure 4 Relative locations of FBG sensors attaching to beam surface.

The propeller-to-beam interaction is particularly relevant to aeroelasticity behavior in a distributed propeller-wing system. Therefore, measuring the propeller slipstream and forces with respect to various positions is necessary. Three miniature six-component balances were installed on the aft motor and propeller to measure various instantaneous propeller forces during low-speed flight circumstances. Data collection began once the rotational speed stabilized since the tests were conducted with an increasing load on the load cell. The mean values, which are derived by averaging the observed parameters over the course of a propeller spin, received particular attention.

The Monarch Model 44 optical tachometer was utilized to confirm the speed settings, and it received a signal from a small white piece of reflective tape put on the propeller root, as illustrated in Figure 3. The test's requirements were met since the rotational speed measurement error was less than 0.1%.[15]. All sensors were collected for 30 seconds at each test site, giving any vibrations brought on by the increased propeller speed time to subside[19]. Additionally, it gave ample time to gather sufficient information for time-averaged aerodynamic forces.

The DC 30V/200A variable output power supply was used to power the three motors, which is sufficient for a steady workload. The torque cell and load cell's voltage outputs were routed through instrument amplifiers to a National Instrument data acquisition module that was mounted in a PCI extension for the instrument platform, where they were then sent into the platform's controller module. The LabView software from National Instruments was then used to record the data.

3 RESULTS AND DISCUSSION

3.1.1 Compared with a clean wing

This section compares the time-domain response results of the clean wing under the same operating conditions with the vertical and horizontal deformation simulated. As previously stated, using an SDT scheme for postprocessing the received fiber optic strain data, the deformation of the wingtip was calculated using the strain-based formulation. The gust generator oscillates to provide a continuous sin gust in the gust wind tunnel test with a 2-degree angle of attack. The working conditions of gust frequency, gust amplitude, rotational speed, and velocity in each case are listed in Table 3.

Table 3 Comparison cases.

case	gust frequency/Hz	gust amplitude/deg	rotation speed/r/min	velocity/m/s
1	2	1	8000	19
2	3	1	8000	19
3	4	1	8000	19

With a fixed freestream velocity of 19 m/s, the time history of wingtip deflection about two directions under varying gust frequencies from 1 to 3 Hz are plotted in Figure 5~Figure 7. It is obviously found that the main resonant frequencies of the wind tunnel test are the same as the gust frequencies. Fortunately, the effect of the propeller is also apparent by comparing in Figure 6e and Figure 6f, where the bending curvature occurs 13 fluctuations when the time history is shortened within 0.1 s. It is a frequency determined by the propeller's rotational speed. When comparing the response of horizontal deformation for the DP-Wing configuration to the clean wing, substantially larger oscillations and an absolute value are seen. This is mostly due to the propeller thrust and torque. The response of vertical amplitude is substantially higher than that at the other two frequencies when the gust frequency equals 2 Hz, which is near to the frequency of the first out-plane bending mode. A similar test result of case-2 is presented in Figure 6a, where the gust frequency tends towards the first in-plane bending mode, where the chordwise deflection increases fast and reaches an extremum. Compared with Figure 5a, Figure 6a, and Figure 7a, it is noted that the equilibrium position decreases with the gust frequency increases for the DP-Wing configuration.

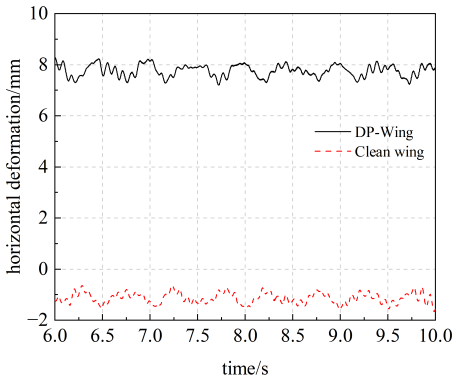

(a) horizontal deformation

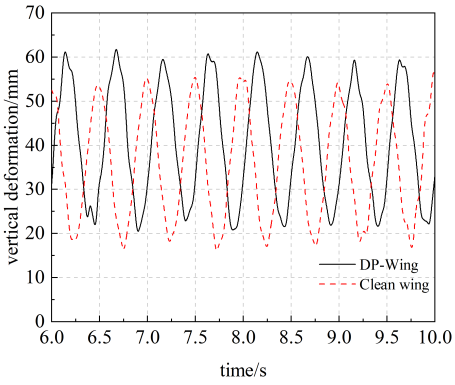

(b) vertical deformation

Figure 5 Response result in time-domain of Case 1

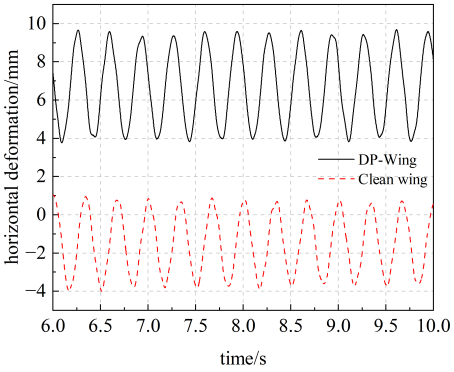

(a) horizontal deformation

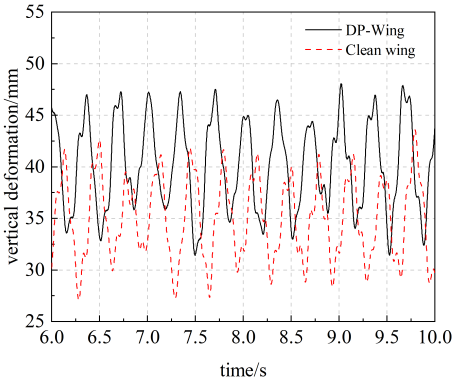

(b) vertical deformation

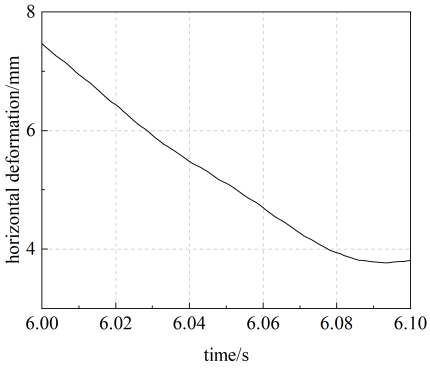

(c) detailed horizontal deformation for DE-wing

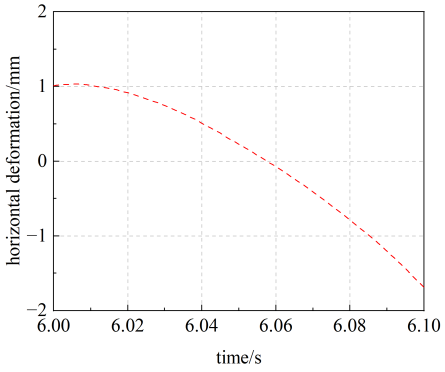

(d) detailed horizontal deformation for clean wing

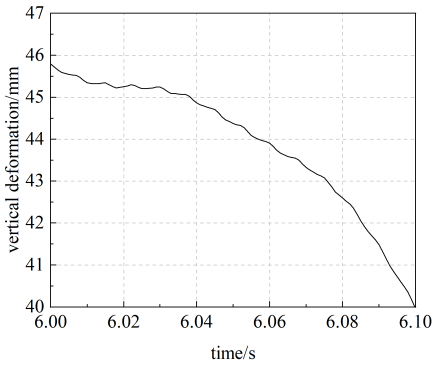

(e) detailed vertical deformation for DE-wing

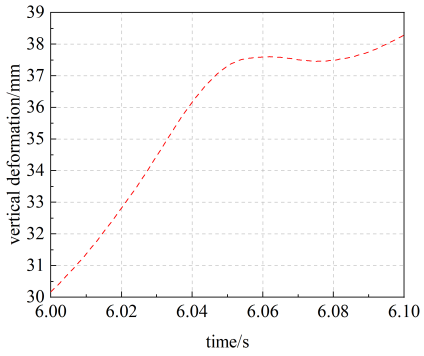

(f) detailed vertical deformation for clean wing

Figure 6 Response result in time-domain of Case 2

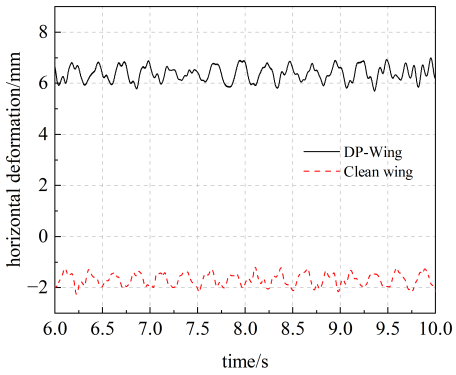

(a) horizontal deformation

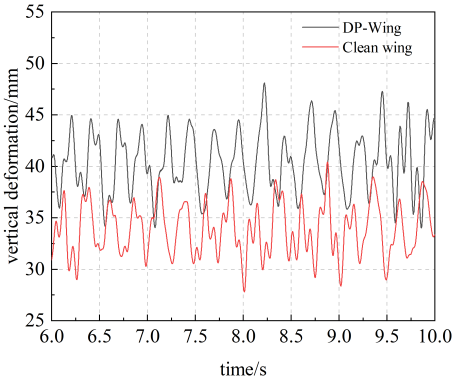

(b) vertical deformation

Figure 7 Response result in time-domain of Case 3

3.1.2 Affected by several working conditions

The complex gust response affected by the distributed propellers pose the dominant challenge for the design of an efficient and safe structure as well as for the analysis using both wind tunnel test method. Table 4 contains a list of each case's operating conditions for gust frequency, gust amplitude, rotational speed, angle of attack, and velocity.

Table 4 Working conditions of gust wind tunnel test.

case	gust frequency/Hz	gust amplitude/deg	rotation speed/r/min	angle of attack/deg	velocity/m/s
4	2	1	8000	0	19
5	3	1	8000	0	19
6	2	2	8000	2	19
7	2	1	8000	2	17
8	2	1	8000	2	19

A comparison of the time domain of wingtip vertical and horizontal deformation under gust frequencies of 2 Hz and 3 Hz is plotted in Figure 8b, which shows the center of fluctuation is located at zero for case-4. This is primarily because the angle of attack is 0 degrees, and the vertical deformation equilibrium position reflect the truly physical phenomenon. The propeller thrust operating in the in-plane direction is the reason for the clearly noticeable relative increase in estimating the horizontal deformation averages. For the horizontal deformation of case-5, the absolute values of deformation is almost 3.5 mm, and the corresponding value is estimated to be 5.5 mm as shown in Figure 6a. The value of the equilibrium position in case-5 is greater than that of case-2, as was indicated in the discussion of the absolute magnitude of the horizontal deformation.

The amplitude of gust does clearly influence the wingtip deformation of DP-Wing configuration, as plotted for a selected time history in Figure 9. The more noticeable variations are discovered when the amplitude of 2 deg is plotted in red, while the amplitude of 1 deg is displayed as a black line. A greater gust amplitude has the potential to significantly alter the wingtip deformation's absolute value. It appears that the equilibrium position for the two cases has not changed despite the conflicting amplitudes. Despite the phase difference, the oscillating amplitudes of the wingtip under different freestream velocities are almost equal, as shown in Figure 10.

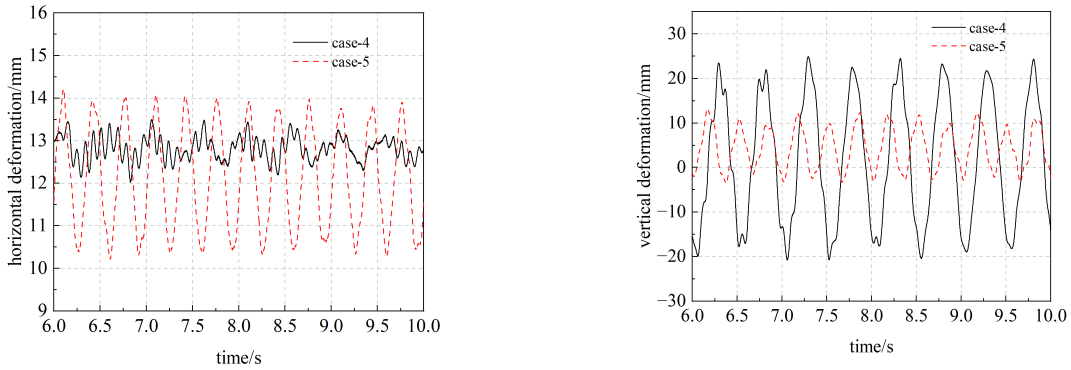

(a) horizontal deformation (b) vertical deformation

Figure 8 Response result in time-domain of case-4 and case-5.

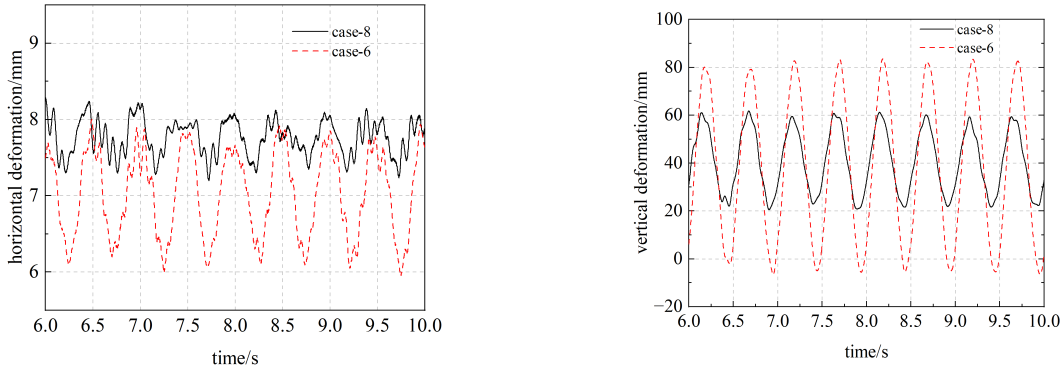

(a) horizontal deformation (b) vertical deformation

Figure 9 Response result in time-domain of case-6 and case-8.

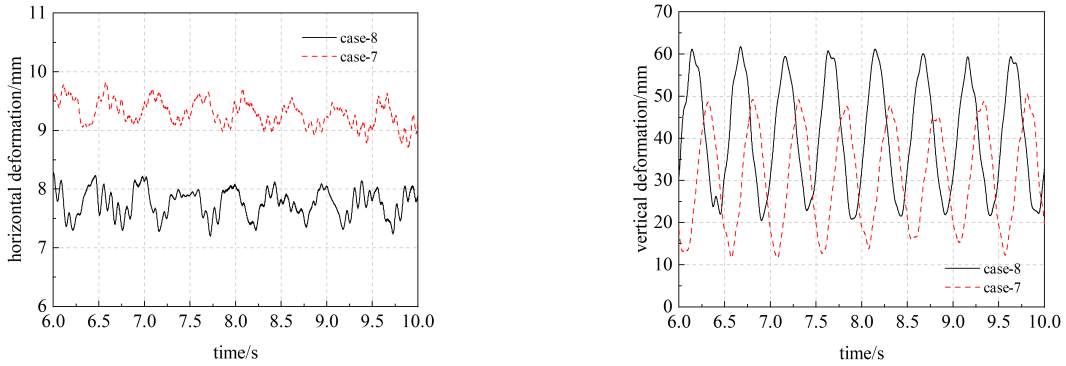

(a) horizontal deformation (b) vertical deformation

Figure 10 Response result in time-domain of case-7 and case-8.

4 CONCLUSIONS

The study presents the development of an efficient distributed propeller-wing measurement system and aeroelastic test model. The method may assist in addressing the difficulties associated with gust alleviation and contribute to a better understanding of the gust response for the distributed propeller-wing configuration. The support system, gust generator and measurement system are described accordingly. A novel fiber optic sensing system has accurately estimated the high-quality time-domain response of both vertical and horizontal deformation through numerical integration. The test findings demonstrate that the gust frequency is reflected in the oscillation frequency of the wingtip deformation. Furthermore, the propeller characteristics are contained in the gust response, which is influenced by the propeller rotation frequency. The three distributed propellers greatly enhance the elastic wing's equilibrium position and gust response amplitude in both directions.

To enable evaluation of the gust response reported in this publication, additional research will be carried out in the next work to examine the degree of coupling between distributed propellers, the wing, and their action mechanism.

REFERENCES

[1] An S. Aeroelastic Design of A Lightweight Distributed Electric Propulsion Aircraft with Flutter and Strength Requirements[D]. Atlanta: Georgia Institute of Technology, 2015.

[2] Baizura B., Quentin B., Murat B., and Emmanuel B. Aerodynamic Model of Propeller–Wing Interaction for Distributed Propeller Aircraft Concept. Proceedings of the Institution of Mechanical Engineers, Part G: Journal of Aerospace Engineering, 2020, 234(10): 1–18.

[3] Helios Prototype Flying Wing[OL]. https://www.nasa.gov/image-article/helios-prototype-flying-wing-2.

[4] Patterson M D, Derlaga J M, Borer N K. High-Lift Propeller System Configuration Selection for NASA's SCEPTOR Distributed Electric Propulsion Flight Demonstrator[C]. 16th AIAA Aviation Technology, Integration, and Operations Conference, Washington, D.C, 2016: AIAA-2016-3922.

[5] Cesnik C.E.S., Su W. Nonlinear Aeroelastic Simulation of X-HALE: A Very Flexible UAV[C]. 49th AIAA Aerospace Sciences Meeting Including the New Horizons Forum and Aerospace Exposition, Orlando, Florida, 2011: AIAA-2011-1226.

[6] Wang K., Zhou Z., Zhu X., et al. Aerodynamic Design of Multi-Propeller/wing Integration at Low Reynolds Numbers[J]. Aerospace Science and Technology, 2019, 84: 1–17.
[7] van Arnhem, N. Unconventional Propeller Airframe Integration for Transport Aircraft Configurations[D]. Ph.D. Dissertation, Delft Univ. of Technology, Delft, The Netherlands, 2022.
[8] William J. F., Robert G. M., Brian F. B., et al. Greased Lightning (GL-10) Flight Testing Campaign[R]. NASA, TM-2017-219643: 1–25.
[9] Nicholas K. B., Joseph M. D., Karen A. D., et al. Comparison of Aero-Propulsive Performance Predictions for Distributed Propulsion Configurations[C]. 55th AIAA Aerospace Sciences Meeting, Grapevine, Texas, 2017: AIAA-2017-0209.
[10] Stoll A. M., Bevirt J., Moore M. D., et al. Fredericks, N. K. Borer. Drag Reduction Through Distributed Electric Propulsion[C]. AIAA Aviation, Atlanta, GA, 2014: AIAA-2014-2851.
[11] Michael D. P., Matthew J. D. Conceptual Design of Electric Aircraft with Distributed Propellers: Multidisciplinary Analysis Needs and Aerodynamic Modeling Development[C]. 55th AIAA Aerospace Sciences Meeting, National Harbor, Maryland, 2014: AIAA-2014-0534.
[12] Teixeira P. C., Cesnik C. E. S. Propeller Effects on the Response of High-Altitude Long-Endurance Aircraft[J]. AIAA Journal, 2019, 57(10): 4328–4342.
[13] Ostuka K., Del C. A., Palacios R. Nonlinear Static and Dynamic Analysis Framework for Very Flexible Multibody Aircraft with Propellers[J]. Journal of Aircraft, 2022, 59(2): 293–306.
[14] Leifsson L., Ko A., Mason W,. et al. Multidisciplinary design optimization of blended-wing-body transport aircraft with distributed propulsion. Aerospace Science and Technology[J], 2013, 25(1): 16–28.
[15] Zhang Z., Xie C., Wang W., et al. An Experimental and Numerical Evaluation of the Aerodynamic Performance of a UAV Propeller Considering Pitch Motion[J]. Drones, 2023, 7, 447: 1–25.
[16] MENG Y., WAN Z., XIE C., et al. Time-domain nonlinear aeroelastic analysis and wind tunnel test of a flexible wing using strain-based beam formulation[J]. Chinese Journal of Aeronautics, 2021, 34(1): 380–396.
[17] An C., Yang C., Xie C., et al. Flutter and gust response analysis of a wing model including geometric nonlinearities based on a modified structural ROM[J]. Chinese Journal of Aeronautics, 2020, 33(1): 48–63.
[18] Meng Y, Xie CC, Wan ZQ. Deformed wing shape prediction using fiber optic strain data. 17th international forum on aeroelasticity and structural dynamics, 2017.
[19] Brian J. G., Mark F. R. Experimental Analysis of Propeller–Wing Interactions for a Micro Air Vehicle[J]. Journal of aircraft, 2009,46(1): 1–9.